Chemical Engineering Journal 474 (2023) 145798

Contents lists available at ScienceDirect

Chemical Engineering Journal

journal homepage: www.elsevier.com/locate/cej

The interplay of sulfate and nitrate triggers abiotic reduction in a hydrogen-based membrane biofilm reactor for antimonate removal

Jingzhou Zhou [a,b,1], Chengyang Wu [c,1], Si Pang [a,b], Lin Yang [a,b], Mengying Yao [a,b], Xiaodi Li [a,b], Siqing Xia [a,b,*], Bruce E. Rittmann [d]

[a] State Key Laboratory of Pollution Control and Resource Reuse, College of Environmental Science and Engineering, Tongji University, Shanghai 200092, China
[b] Shanghai Institute of Pollution Control and Ecological Security, Shanghai 200092, China
[c] School of Environment and Architecture, University of Shanghai for Science and Technology, Shanghai 200093, China
[d] Biodesign Swette Center for Environmental Biotechnology, Arizona State University, Tempe, AZ 85287-5701, United States of America

ARTICLE INFO

Keywords:
Antimony bioremediation
Membrane biofilm reactor
Interaction
Sulfide

ABSTRACT

Sb is classified as a priority pollutant, to control the pollution in aquatic environments of Sb, enhance the understanding of Sb biogeochemical cycle, the effects of sulfate and nitrate on antimonate (Sb(V)) removal in a Hydrogen-Based Membrane Biofilm Reactor (H_2-MBfR) were investigated. With the input of sulfate, the MBfR achieved 90% Sb removal and a removal flux up to 0.76 g Sb/m^2·day. The Sb(V) was reduced to Sb(III), which was primarily Sb_2S_3 solids retained in the biofilm. Furthermore, the mechanism of antimonate reduction shifted from enzymatic reduction with no sulfate input to abiotic reduction based on sulfide produced microbially being the reductant. The subsequent input of nitrate suppressed Sb(V) reduction and removal, along with suppressing sulfate reduction. Nitrate became the dominant electron acceptor, which led to Sb_2S_3 oxidation and the net release of Sb(V) and SO_4^{2-}. This work reinforces that the H_2-MBfR is a promising bioremediation strategy for antimonate removal, and it provides mechanistic insights regarding the impacts of sulfate and nitrate on antimonate reduction and removal.

1. Introduction

Antimony (Sb) is listed as a critical mineral by the U.S. Geological Survey due to its widespread use in flame retardants and lead-acid batteries, as well as an input to semiconductor, textile, and catalyst industries [1,2]. Sb also is a pollutant in aquatic environments and is classified as a priority pollutant by the European Council, the United States Environmental Protection Agency, the Chinese Environmental Protection Agency, and the Japanese Environmental Protection Agency [3].

In antimony mining and smelting, Sb usually appears in surface waters as Sb(V), typically $Sb(OH)_6^-$, at up to 11 ppm Sb, while Sb(III) is not detected [4]. The absence of Sb(III) is associated with it precipitating as Sb_2O_3(s) or Sb_2S_3(s). Compared with Sb(V), Sb (III) is more easily absorbed and removed by centrifugation or filtration [5,6]. Therefore, controlling the state of Sb is crucial for controlling its fate and risk, investigating strategies that reduce Sb(V) to Sb(III) should be effective for removing Sb from water [7–9]. The physicochemical methods such as combining coagulation precipitation and membrane separation process, electrochemical methods, and adsorption methods have been reported to control the Sb pollution [10–12]. While the physicochemical methods are usually high operational costs, and lead to secondary contamination [13]. As a low-cost and environmentally friendly manner, Sb bioremediation was thought to be a promising pathway to control the redox state and reduce Sb(V) to Sb(III) [14].

Microorganisms require an electron donor to reduce Sb(V). Among the bioavailable electron donors, H_2 is especially promising, because H_2 is non-toxic, is relatively inexpensive, leaves no residual organic, and has been applied for microbiological reductions of various many contaminants [15–19]. The low water solubility of H_2 limited its use in water treatment, but this was overcome by using an H_2-based membrane biofilm reactor (H_2-MBfR). In a H_2-MBfR, H_2 diffuses through the walls of non-porous hollow-fiber membranes and is delivered directly to a biofilm attached on the outside surface of the membrane [20,21]. A

* Corresponding author at: State Key Laboratory of Pollution Control and Resource Reuse, College of Environmental Science and Engineering, Tongji University, Shanghai 200092, China.
E-mail address: siqingxia@gmail.com (S. Xia).
[1] Jingzhou Zhou and Chengyang Wu equally contributed to this work.

https://doi.org/10.1016/j.cej.2023.145798
Received 12 June 2023; Received in revised form 26 August 2023; Accepted 31 August 2023
Available online 4 September 2023
1385-8947/

previous work documented Sb(V) reduction and removal in the H_2-MBfR [22]. However, there usually are other coexist ions in the facilized situation might influence the performance. Therefore, the interactions of the coexist matters to the Sb bioremediation need to be clarify, especially for oxidized ions that might also serve as the electron acceptors and compete the electron donor with Sb(V). As it reported the coexist oxidized ions with Sb(V) in mine drainage: e.g., 60–300 mg/L sulfate and up to 10 mg/L nitrate-N [4]. Coexisting sulfate may have a positive impact on Sb removal when sulfate-reducing bacteria (SRB) produce sulfide that precipitates Sb(III) as Sb_2S_3 [23,24]. In contrast, coexisting nitrate may harm Sb(V) reduction and removal in two ways: by directly inhibiting Sb(V) reduction or by oxidizing Sb(III) as the electron donor for denitrification [25,26]. Though these potential relationships among Sb(V), NO_3^-, and SO_4^{2-} have been reported, the effects on microorganisms are not well defined in general [27] and not at all for the H_2-MBfR.

Part of understanding the interactions revolves around reductases able to reduce the three electron acceptors. The respiratory arsenate reductase (ArrAB) mediates dissimilatory Sb(V) reduction [28], and the arsenate reductase ArsC mediates cytoplasmic antimonate reduction [22]. The dissimilatory sulfate-reduction pathway includes a three-step reaction process (Fig. S1): sulfate is first transformed to APS (adenosine 5′-phosphosulfate) from the *sat* gene, and the *aprA* and *aprB* genes encode adenylylsulfate reductase, which converts APS to sulfite. Finally, *dsrA* and *dsrB* drive the transformation from sulfite to sulfide [29]. Revealing which genes are transcribed would help to understand how the coexisting ions affect the microbial community and Sb(V) removal.

In this work, we investigated Sb(V) reduction and Sb's fate in the H_2-MBfR with coexisting sulfate and nitrate. We quantified antimonate-removal kinetics in the H_2-MBfR, identified the antimonate-reduction pathway using transcriptomics, characterized the biofilm's community structure using high-throughput sequencing of the 16S rRNA gene, evaluated the biofilm's morphology with scanning electron microscopy (SEM) and transmission electron microscope (TEM), and revealed the presence of Sb and S solids using electron microscopy and X-ray spectroscopy (XPS).

2. Materials and methods

2.1. Reactor configuration

The MBfR contained two bundles of nonporous polypropylene hollow fibers (Teijin, Japan): The main bundle contained 32 fibers, and the coupon bundle contained 20 fibers for biofilm sampling. The H_2 pressure to the fibers' lumen was regulated at 1.5 atm (absolute) to give a H_2-delivery capacity of 0.366 g H_2/m^2·d [30]. The MBfR was operated at room temperatures (25 ± 1 °C) in a continuous-flow and completely mixed mode: an influent flow rate at 0.29 mL/min and a recirculation rate at 100 mL/min. Configuration details are in **Section S2** of Supplementary Information (SI).

2.2. Startup and operation

Acclimated H_2-oxidizing and autotrophic denitrifying bacteria (detailed description of their enrichment is in **Section S3**) were inoculated into the MBfR. The MBfR was fed with basal salts medium (containing bicarbonate as the inorganic carbon source, phosphate buffer, and trace elements detailed in **Section S3**) that also contained 10 mg/L of Sb(V) (provided as $KSb(OH)_6$, AR, Ourchem, China) and 0, 60, 120, 240, or 240 mg/L of SO_4^{2-} (provided as Na_2SO_4, AR, Sinopharm, China) without NO_3^- in Stages S1, S2, S3, S4, and S6 respectively. Each stage was operating for 15 days, which allowed the effluent to reach steady state. In Stage S5, 10 mg /L NO_3^--N (provided as $NaNO_3$, AR, Sinopharm, China) was added in addition to 10 mg /L of Sb(V) and 240 mg /L of SO_4^{2-}. Stage S5 was operated 30 days.

The batch test was carried out after S6 using the basal salts media contained 240 mg/L of SO_4^{2-} (provided as Na_2SO_4, AR, Sinopharm, China) and 10, 20, 50 mg/L of Sb(V) (provided as $KSb(OH)_6$, AR, Ourchem, China) individually in the MBfR. The samples were taken at 0, 20, 30, 45, 60, 75, 105, 135, 165, and 225 min.

2.3. Chemical analyses

Effluent samples were collected and filtered through a 0.22-μm membrane filter (25-mm PES, Titan, China) daily. To measure the concentrations of Sb(V), SO_4^{2-}, NO_3^-, and NO_2^-, water samples were analyzed with an Ion Chromatograph (Dionex Aquion, USA) with an AS11HC column and AG11HC precolumn. The eluent of IC was set as 15 mM KOH at a 1 mL/min flow rate. The concentration of Sb(III) was assayed using an HPLC-ICP-MS (Agilent LC1200-ICPMS 7700, Agilent, USA). An anion exchange column (PRP-X100, 4.1 × 150 mm, 10 μm, Hamilton, Switzerland) was equipped with HPLC. The mobile phase were applied as EDTA (20 mM) and 2 mM potassium hydrogen-phthalate at pH 4.5, the flow rate was set as 1 mL/ min. The injection samples were 10 μL water samples collected from MBfR that were diluted 100-fold with ultrapure water[7]. The concentration of ammonium-nitrogen (NH_4^+-N) was determined by the standard methods [31].

Removal fluxes (g/m^2·d) were calculated according to

$$J = \frac{Q(S_0 - S)}{A} \quad (1)$$

where S_0 and S are the influent and effluent ions concentration (g/L), Q is the influent flow rate to the MBfR (L/d), and A is the membrane surface area (m^2). To evaluate the demand of maximum H_2 flux in theoretical, the substrate-mass fluxes were converted to electron-equivalent fluxes based on the maximum electron-equivalent fluxes in theory that Sb(V) being reduced to Sb(III) (2 e^- eq/mol), SO_4^{2-} to H_2S (8 e^- eq/mol), and NO_3^- to N_2 (5 e^- eq/mol).

2.4. Biofilm transcriptomics and community structure analysis

Biofilm samples were collected at the end of S2, S4, S5, and S6. Two 18-cm-long sections from a coupon fiber were cut off for DNA extraction and RNA separation. After sampling, the open end of the remaining fiber was tied with 2 knots to avoid H_2 leakage.

Total RNA was extracted using a TaKaRa MiniBEST Universal RNA Extraction Kit (TaKaRa,Japan), and it was reverse transcribed to cDNA following the instructions of the PrimeScript™ RT reagent Kit with gDNA Eraser (Perfect Real Time, TaKaRa, Japan) immediately [32]. The primer pairs aprA-1-F / aprA-5-R, DSRp2060F / DSR4R, arrA-CVF / arrA-CVR,amlt-42-f / amlt-376-r and smrc-42-f / smrc-376-r, 16SF / 16SR were used to confirm the change of the genes of target,16S rRNA [33], *arrA* [34], *arsC* [35], *aprA*, *dsrB*,[36], respectively, for real-time qPCR (Details in **Section S4**). All qPCR analyses were performed using the CFX Connect™ Real-Time PCR System (Bio-Rad, USA). The qPCR amplification mixture (20 μL) was prepared using 10 μL SYBR Premix Ex Taq™ (Takara, Japan), 1 μL of each forward and reverse primer (20 mM), 1 μL of cDNA template, and 7 μL of RNase-free water (Takara, Japan) according to the manufacturer's instructions. All RT-qPCR assays were carried out in triplicate. Standard dilution curves were generated for each pair of primers. The fold change (relative expression level) of target genes was measured using the the $2^{-\Delta\Delta CT}$ method with using partial 16S rRNA gene as a reference gene and taking S2 as a control stage. Specifically, the formula is described as:

$$2^{-\Delta\Delta CT}\ \text{method} = 2^{-(CtSX\text{-}CtRSX)\text{-}(CtS2\text{-}CtRS2)}$$

Ct_{SX} and Ct_{S2} refer to the Ct values of the target gene in SX(X = 4,5,6) and S2, respectively. Ct_{RSX} and Ct_{RS2} refer to the Ct values of the reference gene in SX(X = 4,5,6) and S2, respectively [37,38].

Genomic DNA was extracted with a DNeasy PowerBiofilm Kit (QIAGEN GmbH, Germany) according to the manufacturer's

specification. The DNA concentration was measured using NanoDrop 2000 (Thermo Fisher Scientific, USA).

PCR primers 338F and 806R were applied to amplify the V3-V4 region of the bacteria's 16S rRNA gene [39]. The Illumina MiSeq PE300 platform (Majorbio Bio-pharm Technology Co., Ltd, Shanghai, China) was used to sequence the amplicons. Sequence data were analyzed on the online platform of Majorbio ISanger Cloud Platform. Qualified sequences were clustered into operational taxonomic units (OTUs) at 97% similarity using the Uparse software version 11 [40]. Based on the OTU information, the richness and evenness of microbial species were evaluated.

2.5. Biofilm imagining and solid-state characterization

At the end of S6, two ~ 3-cm-long coupon fibers were cut off for scanning electron microscopy (SEM; Zeiss Sigma 300, German) and transmission electron microscopy (TEM; JEOL JEM 2100F, Japan) equipped with energy dispersive X-ray spectroscopy (EDS).

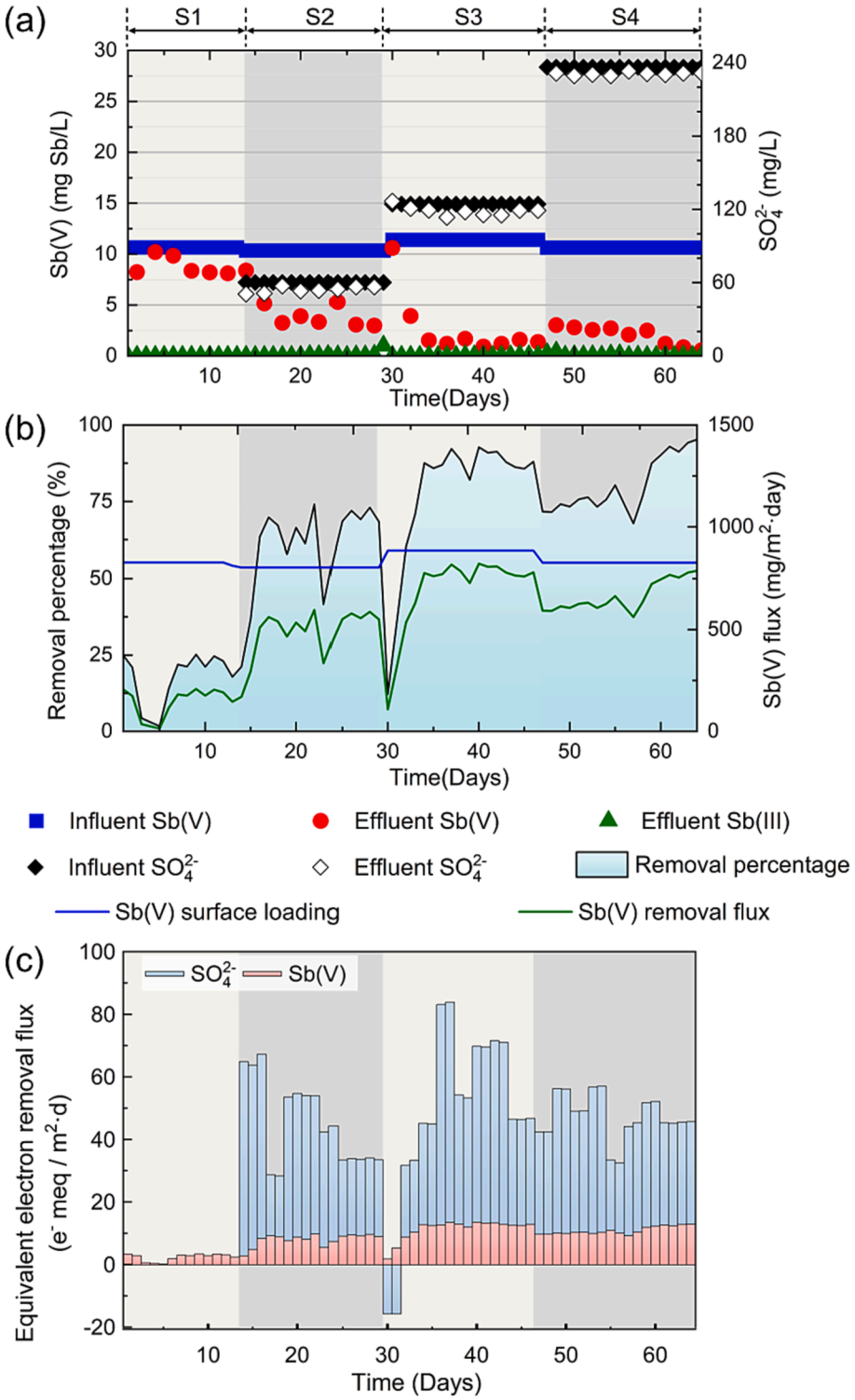

Fig. 1. Sb(V) and SO_4^{2-} removals for Stages 1–4 of H_2-MBfR operation. The maximum H_2-delivery flux was 366 e^- meq/m^2-day.

Twenty main-column fibers were desiccated in a freeze-dryer (FD-1A-50, BILON, China) to recover the solid-phase reduction products. X-ray photoelectron spectroscopy (XPS) was applied to analyze the valence state of reduction production through a Thermo Scientific K-Alpha (ThermoFisher, USA). X-ray diffraction (XRD) was applied to analyze the structure of reduction production using an X-ray Diffractometer (Rigaku SmartLab SE, Japan) with Cu- Kα radiation (40 kV, 40 mA).

3. Results and discussion

3.1. The effect of sulfate on Sb(V) removal

Fig. 1**a** shows the daily influent and effluent concentrations of Sb(V), Sb(III), and SO_4^{2-} during S1 to S4. The Sb(V)-removal percentages, -surface loadings, and -removal fluxes are in Fig. 1**b**, with calculated electron-equivalent fluxes in Fig. 1**c**.

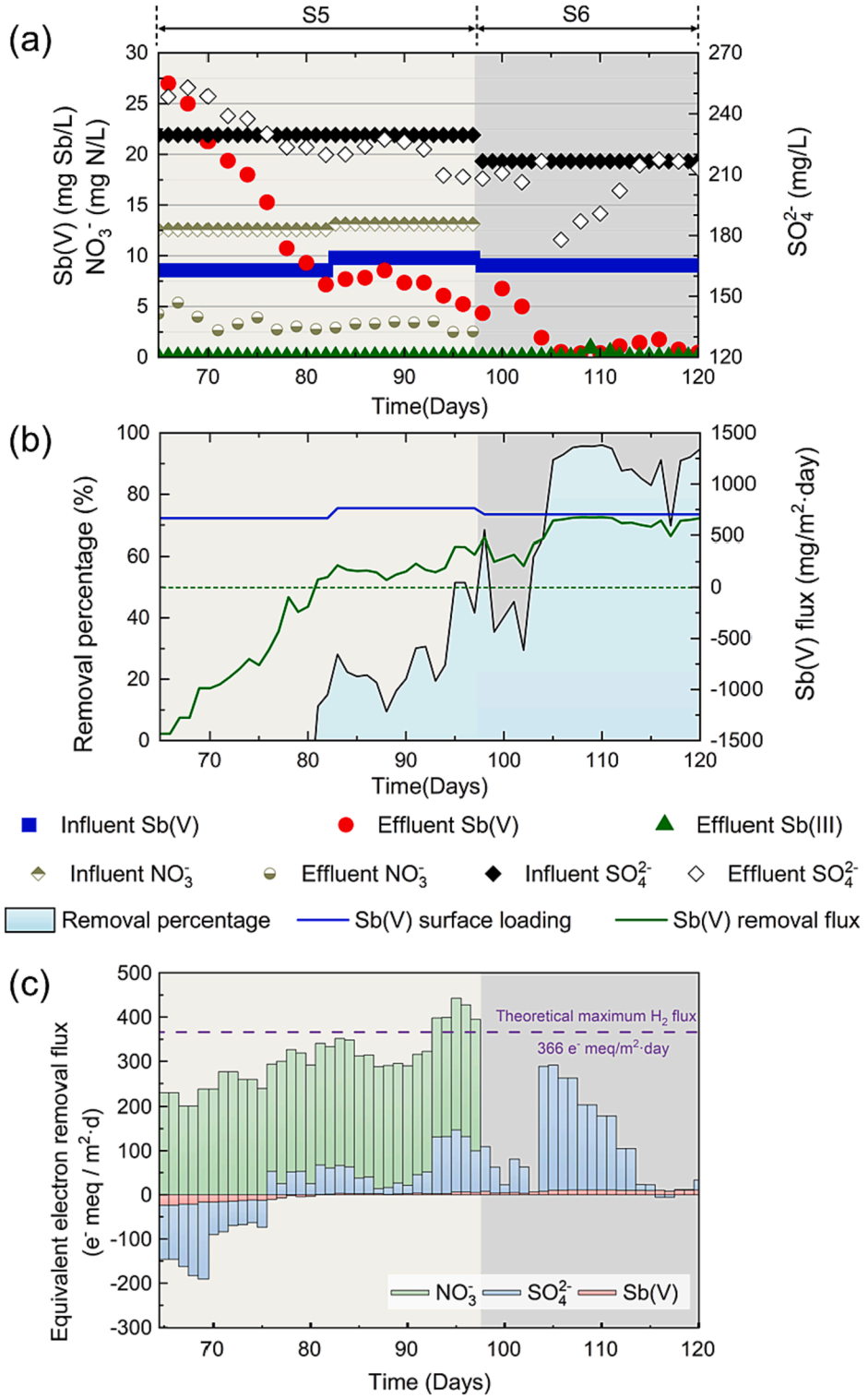

Fig. 2. Sb(V), SO_4^{2-}, and NO_3^- removals for Stages S5-S6 of H_2-MBfR operation. Nitrite was<0.3 mg N/L (not shown).

When Sb(V) was the sole electron acceptor in S1, the average Sb(V)-removal percentage was only 23% at the end of S1′s 14 days. When 60 mg/L of SO_4^{2-} was introduced to the influent in S2, the Sb(V)-removal percentage increased to 60%, giving an average Sb(V)-removal flux of 0.49 g/m^2·day. In S3, the concentration of SO_4^{2-} was increased to 120 mg/L, and the Sb(V)-removal percentage increased to 85%, with an Sb (V)-removal flux of 0.75 g/m^2·day. When 240 mg/L SO_4^{2-} was fed during S4, the Sb(V)-removal flux decreased to 0.64 g/m^2·day at first due to the increase of the influent SO_4^{2-} concentration, after a period of acclimation it increased to 90% for days 59 to 64 (flux of 0.76 g/m^2·day). In summary, the increase of SO_4^{2-} loading enhanced the Sb(V)-removal, the Sb(V)-removal percentage increased with the increase of SO_4^{2-} loading from S1 to S4. Furthermore, the average effluent concentration of Sb(III) from Day14 to 64 was<0.6 mg/L, a major improvement over previous research with Sb(V) as sole electron acceptor in MBfR, in which most Sb (III)(~50%-89%) was discharged in effluent [5,22], which suggested the input of the sulfate also enhanced the total Sb removal.

The electron-equivalent fluxes (Fig. 1c) were less than the theoretical maximum H_2 flux (366 e^- meq/m^2·day = 366 mg H_2/m^2·day) during S1 to S4, thus, the electron-donor supply was sufficient. Sulfate reduction dominated Sb(V) reduction as an electron sink. The lack of Sb in the effluent and strong sulfate reduction support that Sb(III) was retained in the biofilms as Sb_2S_3 or other Sb-S complex when SO_4^{2-} was present in the influent.

3.2. Impact of NO_3^- On Sb(V) and SO_4^{2-} reductions

Nitrate was added at 10 mg N/L in S5 and then removed from the influent in S6. The concentrations of Sb(V), Sb(III), SO_4^{2-}, and NO_3^- in influent and effluent, surface loadings, removal fluxes, and electron-equivalent fluxes are summarized in Fig. 2.

In the first 10 days of S5, the Sb(V)-removal and the sulfate-removal presented negative values, which support that introducing nitrate led to oxidation of Sb_2S_3 solids that had accumulated in the biofilm. The effluent NO_3^- was 5.5 mg N/L (average of Days 65 to 69), but decreased to 3.1 mg/L (average of Days 70 to 97). By Day 80, the Sb(V)-removal flux returned to positive value and then continued to increase. Nonetheless, the average Sb(V)-removal flux for Days 80 to 97 was only 0.19 g/m^2·day, or 38% of the flux in S4 (0.50 g/m^2·day). NO_2^- in the effluent was<0.3 mg N/L during S5 and NH_4^+-N was under the detection limit (data not shown), indicating that NO_3^- was most likely reduced to N_2.

Over S5 (Days 65 to 92), the net electron-equivalent fluxes remained smaller than the maximum electron-equivalent delivery flux of H_2. However, at the end of S5 (Days 93 to 97), the total electron-equivalent flux for reductions of NO_3^- and SO_4^{2-} exceeded the theoretical maximum H_2 flux as the SO_4^{2-}- and NO_3^--removal fluxes became larger. Having a net reduction flux greater than the H_2-delivery capacity suggests the possibility of some S^0 was produced and retained, which would lead to an electron balance. The dominant electron-equivalent flux in S5 was for NO_3^- reduction, and this was accompanied by diminished electron-equivalent fluxes for SO_4^{2-} and Sb(V) reductions. Thus, denitrification inhibited other reduction process due either to competition for electron donor, direct inhibition, or both.

In S6, NO_3^- was removed from the influent, and the SO_4^{2-} and Sb(V) removal fluxes increased at Day 104. However, the SO_4^{2-}-removal flux began decreasing from Day 105, eventually declining to close to zero. The Sb(V)-removal flux reached a relatively stable state from Days 105 to 120: 0.64 g/m^2·day, or 128% of S4 and 337% of S5.

Overall, S5 and S6 demonstrate that nitrate inhibited Sb(V) removal, even though the sulfate-removal flux increased. It appears that nitrate exposure led to Sb_2S_3 oxidation coupled to NO_3^- reduction. This phenomenon could be a good means to release Sb(III) that has accumulated in biofilm for Sb recycling, but it is deleterious for Sb(V) reduction and removal.

3.3. Route of Sb(V) reduction in the MBfR

3.3.1. Functional gene expression

Fig. 3 presents the relative mRNA expression levels for *arrA*, *arsC*, *aprA*, and *dsrB* genes during S2, S4, S5, and S6. From S2 to S4, sulfate suppressed the expression of the *arrA* gene ($p < 0.0001$). In S5, nitrate further suppressed the expression of the *arrA* gene ($p < 0.01$). In S6, removing nitrate did not lead to recovery of *arrA* gene expression. These trends indicate that sulfate and nitrate suppressed the expression of the *arrA* gene, which means that dissimilatory antimonate reduction was down-regulated. The expression of the *arsC* gene also was suppressed due to the input of sulfate ($p < 0.1$), but the addition of nitrate up-regulated *arsC*-gene expression ($p < 0.001$) from S4 to S5. This may have been related to the increased Sb(V) surface loading and greater oxidation of Sb(III) to Sb(V).

The simultaneous changes in the expression of the *arrA* and *arsC* genes indicate that dissimilatory and cytoplasmic Sb(V) reductions were down-regulated by the addition of sulfate. However, the Sb(V)-removal fluxes increased, which implies that Sb(V) reduction shifted away from a route mediated by ArrA or ArsC when the input of sulfate increased.

The *aprA* and *dsrB* genes were up-regulated with the increasement of influent sulfate, which corresponded to greater sulfate reduction. Therefore, an alternative mechanism is proposed: abiotic reduction of Sb (V) in which sulfide, produced microbially, is the reductant for a non-enzymatic reaction [24].

3.3.2. Sb(V) removal kinetics

Fig. S3 shows the plots of ln[$Sb(OH)_6^-$] versus time for the removal of $Sb(OH)_6^-$ in the presence of 240 mg/L SO_4^{2-} and with initial concentrations of [$Sb(OH)_6^-$] at 50, 20, or 10 mg Sb/L in the H_2-MBfR. The first-order rate constants for the reduction of Sb(V) were similar, and the average first-order rate was $k' = 11.0 \pm 2.1 \times 10^{-3}$ min^{-1}. This rate constant is larger than reported using dissolved sulfide to reduce Sb(V) in an abiotic batch test [41]. This faster rate supports the value of using H_2-MBfR to produce sulfide for abiotic Sb(V) reduction.

3.4. Characteristics of the biofilm and reduction products

3.4.1. Biofilm community

Fig. 4 presents the changes of community structure in S2, S4, S5, and S6. *Desulfovibrio* and *norank_f_Sutterellaceae* are sulfate-reducing bacteria (SRB) [42,43] that increased from S2 to S4, decreased in S5, and recovered in S6 with the removal of input nitrate. The sulfate-removal fluxes and the *aprA* and *dsrB* gene-expression levels changed similarly and in concordance with the increased sulfate reduction by SRB in S2, S4, and S6. Meanwhile, the change of SRB abundance is simultaneously with the change of Sb(V)-removal, which supported the abiotic reduction of Sb(V) with sulfide, produced microbially. The upregulation of the *arsC* gene in S5 was accompanied by increases in *unclassified_f_Rhodocyclaceae* and *g_norank_f_Pleomorphomonadacea*, which are Sb-resistant bacteria (SbRB) that possess the *arsC* gene [22]. The input of nitrate in S5 affected the biofilm community structure significantly, leading to a domination by autotrophic denitrifiers *Zoogloea* and *Terrimonas* [44,45]. In contrast, the introduction of nitrate coincided with decreases in heterotrophic *Azonexus*, *norank_f_AKYH767*, and *Methylocystis* [46,47]. The increase in heterotrophic *norank_f_PHOS-HE36* in S6 may have been associated with their capacity for sulfur oxidation [48].

3.4.2. Biofilm morphology

The biofilm was occupied by bacilli and cocci (Fig. 5**a and 5b**) that were surrounding by nanoparticles (Fig. 5**a, 5b, and 5c**). The mean size of the 196 nanoparticles in Fig. 5**c** is 71.5 nm and conforms to a log-normal distribution (D'Agostino & Pearson test, $p = 0.1836$).

3.4.3. Reduction-product characteristics

EDS patterns (Fig. S4**b**) show that Sb and S were the main elements in

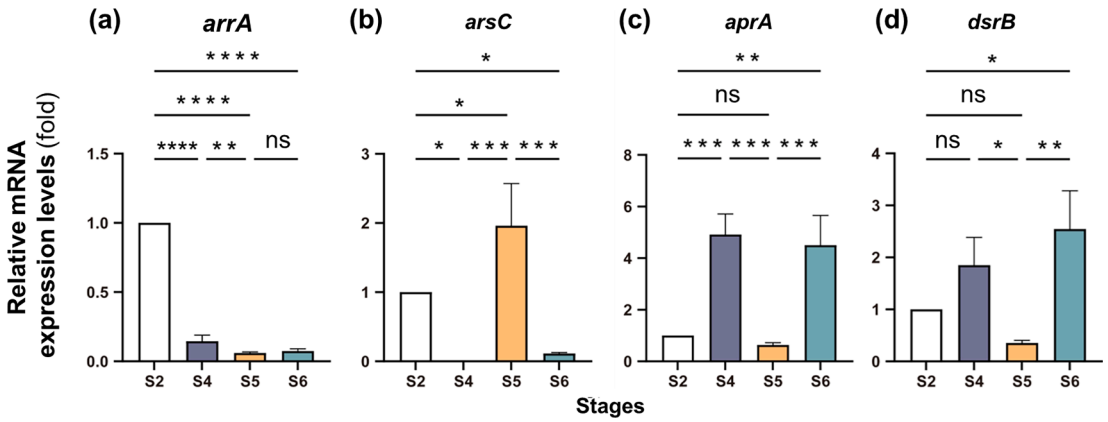

Fig. 3. Relative expression levels of functional genes during the operating period, based on the mean values from three replicate RT-qPCR reactions.

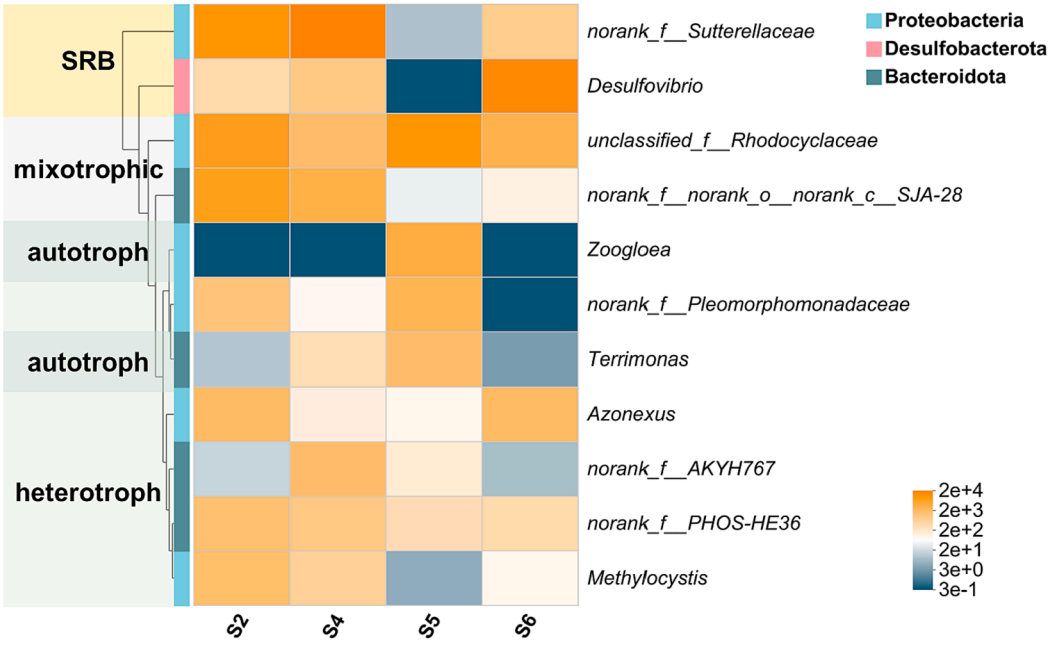

Fig. 4. Heatmap of bacterial genera that occupied ≥ 1.5% of all sequences with stages S2,S4,S5, and S6. The OTU abundance of different species in the sample is displayed through the color gradient.

the biofilms beyond the basic C, N, and O elements in cells. XPS patterns document that Sb(III) was the predominant oxidation state for the Sb precipitates (Fig. 5**e**). S(-II) was the predominant oxidation state for S, as well a small amount of S^0 was present (Fig. 5**f**). The EDS and XPS results support that the precipitates were composed primarily of an Sb(III)-S complex. XRD spectra (Fig. S5) indicated the Sb(III)-S complex contained Sb_2S_3 and Sb_2O_3. In summary, the reduction product by the biofilm included a mixture of Sb_2S_3 and Sb_2O_3.

3.5. The interactions of sulfate and nitrate to the antimonate removal in H_2-MBfR

Fig. 6 summarizes the mechanisms acting in the MBfR biofilm exposed to oxidized Sb, S, and N. With the input of the sulfate, the biofilm's dissimilatory and cytoplasmic antimonate reductions were suppressed (Fig. 3**a and 3b**), but the bioreduction of sulfate driven by H_2 dominated the biofilm's activity (Fig. 3**c and 3d**). H_2-based sulfate reduction is described by **eq 1** [49]:

$$SO_4^{2-} + 4H_2 + H^+ \rightarrow HS^- + 4H_2O \quad \Delta G^{0'} = -19.0\ \mathrm{kJ}/mole^- \tag{1}$$

With strong sulfate reduction, Sb(V) reduction and removal were linked to the S cycle, as described by **eqs 2–5** [24,50]:

$$Sb(OH)_6^- + HS^- \rightarrow Sb(OH)_3 + S^0 + H_2O + 2OH^- \tag{2}$$

$$3Sb(OH)_6^- + S^0 \rightarrow 3Sb(OH)_3 + SO_4^{2-} + 4H_2O + OH^- \tag{3}$$

$$2Sb(OH)_3 + 3HS^- \rightarrow Sb_2S_3(s) + H_2O \tag{4}$$

$$2Sb(OH)_3 \rightarrow Sb_2O_3(s) + 3H_2O \tag{5}$$

When the large input of sulfate shifted the biofilm to reduce SO_4^{2-} instead of Sb(V), but the sulfide produced microbially led to abiotic Sb (V) reduction and enhanced Sb(V) and total Sb removal. The fates of Sb and S were illustrated by **eqs 1–5**. First, the input of sulfate led a hydrogen-based sulfate bioreduction and the accumulation of sulfide. Then the sulfide reduced the Sb(V) to Sb(III), generating S^0 as an intermediate and SO_4^{2-} as a terminal product. Finally, the Sb(III) transformed to Sb(III)-S complex like Sb_2S_3 by the reactions with excess sulfide or Sb_2O_3 directly. The input of the nitrate induced anaerobic Sb (III) oxidation coupled to nitrate reduction and dissolution as Sb(V).

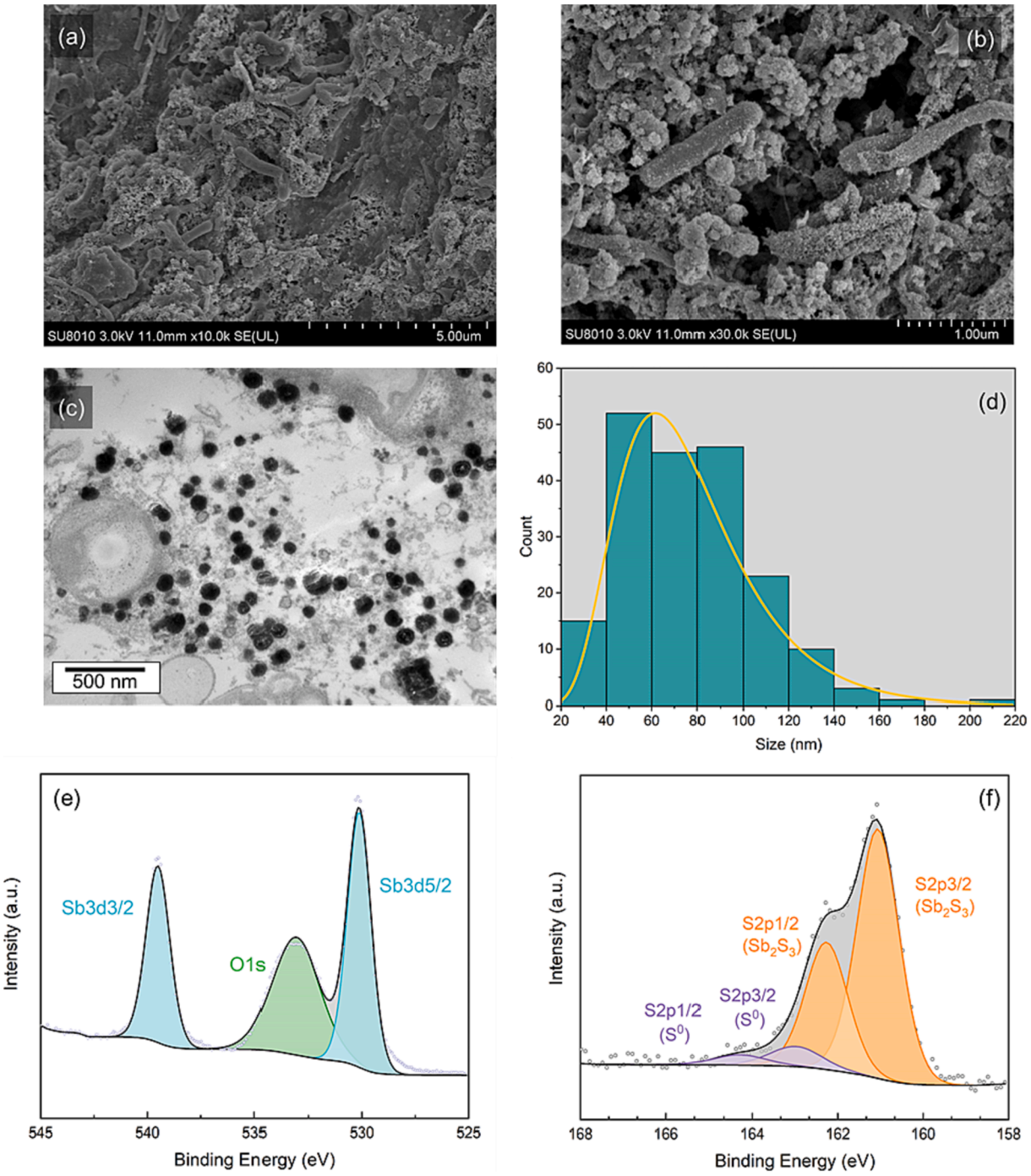

Fig. 5. SEM was observed at 10-k magnification (a), and 30-k magnification (b). TEM was observed at 30-k magnification (c). Size distribution of the nanoparticles (d). XPS patterns towards for 525–545 eV (e) and 158–168 eV (f) of precipitates in the biofilm.

Thus, solid Sb(III) and S(-II) retained in the biofilm were released as Sb (V) and SO_4^{2-}. The release of Sb(V) seemed to promote cytoplasmic antimonate reduction. And removing nitrate allowed antimonate removal to recover over about 7 days.

4. Conclusion

Sulfate and nitrate affected antimonate reduction and removal in a H_2-MBfR in complex ways. Increasing the input of sulfate led to greater Sb(V) reduction and removal, but the mechanism of Sb(V) reduction shifted from enzymatic reduction with no sulfate input to abiotic reduction based on sulfide produced microbially being the reductant. Sb (III) was primarily Sb_2S_3 solids that were retained in the biofilm. Sb(V) reduction and removal were suppressed by the input of nitrate. Furthermore, nitrate served as an electron acceptor for the oxidation of Sb_2S_3 solids and the net release of Sb(V) and SO_4^{2-}.

This work illuminated the impacts of sulfate and nitrate on antimonate reduction and removal. Sulfate reduction enhanced antimonate removal in the H_2-MBfR, but nitrate suppressed sulfate and antimonate removals. The interplay of enzymatic and abiotic reductions of Sb(V) and the fate of Sb(III) in the biofilm are promising research avenues for enhancing fundamental understanding of interactions among electron acceptors and for improving the reliability of microbiological removal of antimonate. For the further research, whether more Sb(V) reducing

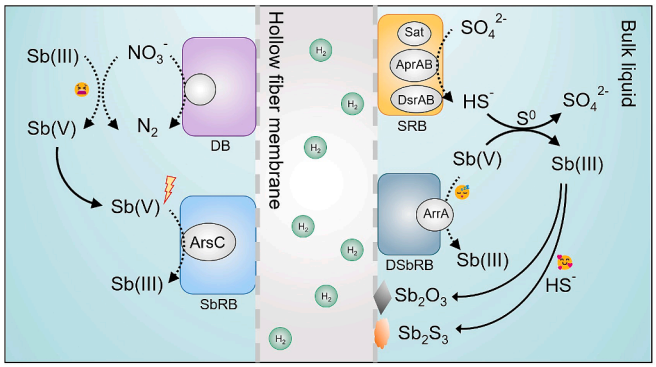

Fig. 6. Schematic representation of the impacts that sulfate and nitrate have on antimonate reduction and removal in the biofilm of an H_2-MBfR. Solid lines (—) indicates abiotic processes. Dotted line (···) indicates the enzymatic reactions. SRB: sulfate-reducing bacteria, DSbRB: Dissimilatory Sb-reduction bacteria, DB: Denitrifying bacteria, SbRB: Sb-resistant bacteria.

enzymatic pathways existing, further insights of the interactions between nitrate and the Sb bioremediation, the effects of more specific operation conditions like different Sb or SO_4^{2-} concentrations, the pressure of H_2 apply, temperature, pH, hydraulic retention time are recommended to be studied to enhance the understanding of Sb bioremediation.

Declaration of Competing Interest

The authors declare that they have no known competing financial interests or personal relationships that could have appeared to influence the work reported in this paper.

Data availability

Data will be made available on request.

Acknowledgments

This work is supported by the National Key Project of Research and Development Plan of China (Grant No. 2021YFC3201300) and Shanghai Leading Talent Project (Grant No. 070).

Appendix A. Supplementary data

Supplementary data to this article can be found online at https://doi.org/10.1016/j.cej.2023.145798.

References

[1] A.C. Scheinost, A. Rossberg, D. Vantelon, I. Xifra, R. Kretzschmar, A.-K. Leuz, H. Funke, C.A. Johnson, Quantitative antimony speciation in shooting-range soils by EXAFS spectroscopy, Geochim. Cosmochim. Acta 70 (2006) 3299–3312, https://doi.org/10.1016/j.gca.2006.03.020.

[2] Mineral commodity summaries 2023, U.S. Geological Survey, 2023. https://pubs.er.usgs.gov/publication/mcs2023 (accessed February 15, 2023).

[3] M. He, N. Wang, X. Long, C. Zhang, C. Ma, Q. Zhong, A. Wang, Y. Wang, A. Pervaiz, J. Shan, Antimony speciation in the environment: Recent advances in understanding the biogeochemical processes and ecological effects, J. Environ. Sci. 75 (2019) 14–39, https://doi.org/10.1016/j.jes.2018.05.023.

[4] F. Liu, X.C. Le, A. McKnight-Whitford, Y. Xia, F. Wu, E. Elswick, C.C. Johnson, C. Zhu, Antimony speciation and contamination of waters in the Xikuangshan antimony mining and smelting area, China, Environ. Geochem. Health 32 (2010) 401–413, https://doi.org/10.1007/s10653-010-9284-z.

[5] C.-Y. Lai, Q.-Y. Dong, B.E. Rittmann, H.-P. Zhao, Bioreduction of Antimonate by Anaerobic Methane Oxidation in a Membrane Biofilm Batch Reactor, Environ. Sci. Tech. 52 (2018) 8693–8700, https://doi.org/10.1021/acs.est.8b02035.

[6] A.V. Zotov, N.D. Shikina, N.N. Akinfiev, Thermodynamic properties of the Sb(III) hydroxide complex Sb(OH)3(aq) at hydrothermal conditions, Geochim. Cosmochim. Acta 67 (2003) 1821–1836, https://doi.org/10.1016/S0016-7037(02)01281-4.

[7] C.-Y. Lai, L.-L. Wen, Y. Zhang, S.-S. Luo, Q.-Y. Wang, Y.-H. Luo, R. Chen, X. Yang, B. E. Rittmann, H.-P. Zhao, Autotrophic antimonate bio-reduction using hydrogen as the electron donor, Water Res. 88 (2016) 467–474, https://doi.org/10.1016/j.watres.2015.10.042.

[8] T.R. Kulp, L.G. Miller, F. Braiotta, S.M. Webb, B.D. Kocar, J.S. Blum, R. S. Oremland, Microbiological Reduction of Sb(V) in Anoxic Freshwater Sediments, Environ. Sci. Tech. 48 (2014) 218–226, https://doi.org/10.1021/es403312j.

[9] C.A. Abin, J.T. Hollibaugh, Dissimilatory Antimonate Reduction and Production of Antimony Trioxide Microcrystals by a Novel Microorganism, Environ. Sci. Tech. 48 (2014) 681–688, https://doi.org/10.1021/es404098z.

[10] D. You, X. Min, L. Liu, Z. Ren, X. Xiao, S.G. Pavlostathis, J. Luo, X. Luo, New insight on the adsorption capacity of metallogels for antimonite and antimonate removal: From experimental to theoretical study, J. Hazard. Mater. 346 (2018) 218–225, https://doi.org/10.1016/j.jhazmat.2017.12.035.

[11] Y. Ren, W. Zheng, S. Li, Y. Liu, Atomic H*-mediated electrochemical removal of low concentration antimonite and recovery of antimony from water, J. Hazard. Mater. 445 (2023), 130520, https://doi.org/10.1016/j.jhazmat.2022.130520.

[12] M. Yuan, Z. Gu, M. Minale, S. Xia, J. Zhao, X. Wang, Simultaneous adsorption and oxidation of Sb(III) from water by the pH-sensitive superabsorbent polymer hydrogel incorporated with Fe-Mn binary oxides composite, J. Hazard. Mater. 423 (2022), 127013, https://doi.org/10.1016/j.jhazmat.2021.127013.

[13] Y. Zhang, C. Ding, D. Gong, Y. Deng, Y. Huang, J. Zheng, S. Xiong, R. Tang, Y. Wang, L. Su, A review of the environmental chemical behavior, detection and treatment of antimony, Environ. Technol. Innov. 24 (2021), 102026, https://doi.org/10.1016/j.eti.2021.102026.

[14] V.K. Nguyen, W. Choi, Y. Park, J. Yu, T. Lee, Characterization of diversified Sb(V)-reducing bacterial communities by various organic or inorganic electron donors, Bioresour. Technol. 250 (2018) 239–246, https://doi.org/10.1016/j.biortech.2017.11.044.

[15] A. Ontiveros-Valencia, C. Zhou, H.-P. Zhao, R. Krajmalnik-Brown, Y. Tang, B. E. Rittmann, Managing microbial communities in membrane biofilm reactors, Appl. Microbiol. Biotechnol. 102 (2018) 9003–9014, https://doi.org/10.1007/s00253-018-9293-x.

[16] B.E. Rittmann, P.L. McCarty, Environmental biotechnology : principles and applications, McGraw-Hill Book Co, New York, 2020. http://core.ac.uk/display/39853960 (accessed November 5, 2021).

[17] C. Zhou, A. Ontiveros-Valencia, R. Nerenberg, Y. Tang, D. Friese, R. Krajmalnik-Brown, B.E. Rittmann, Hydrogenotrophic Microbial Reduction of Oxyanions With the Membrane Biofilm Reactor, Front. Microbiol. 9 (2019). https://www.frontiersin.org/article/10.3389/fmicb.2018.03268 (accessed May 10, 2022).

[18] A. Hassanpouryouzband, E. Joonaki, M. Vasheghani Farahani, S. Takeya, C. Ruppel, J. Yang, N.J. English, J.M. Schicks, K. Edlmann, H. Mehrabian, Z. M. Aman, B. Tohidi, Gas hydrates in sustainable chemistry, Chem. Soc. Rev. 49 (2020) 5225–5309, https://doi.org/10.1039/C8CS00989A.

[19] A. Hassanpouryouzband, K. Adie, T. Cowen, E.M. Thaysen, N. Heinemann, I. B. Butler, M. Wilkinson, K. Edlmann, Geological Hydrogen Storage: Geochemical Reactivity of Hydrogen with Sandstone Reservoirs, ACS Energy Lett. 7 (2022) 2203–2210, https://doi.org/10.1021/acsenergylett.2c01024.

[20] C. Wu, L. Zhou, C. Zhou, Y. Zhou, S. Xia, B.E. Rittmann, Co-removal of 2,4-dichlorophenol and nitrate using a palladized biofilm: Denitrification-promoted microbial mineralization following catalytic dechlorination, J. Hazard. Mater. 422 (2022), 126916, https://doi.org/10.1016/j.jhazmat.2021.126916.

[21] Z. Li, L. Ren, Y. Qiao, X. Li, J. Zheng, J. Ma, Z. Wang, Recent advances in membrane biofilm reactor for micropollutants removal: Fundamentals, performance and microbial communities, Bioresour. Technol. 343 (2022), 126139, https://doi.org/10.1016/j.biortech.2021.126139.

[22] J. Zhou, C. Wu, S. Pang, L. Yang, M. Yao, X. Li, S. Xia, B.E. Rittmann, Dissimilatory and Cytoplasmic Antimonate Reductions in a Hydrogen-Based Membrane Biofilm Reactor, Environ. Sci. Tech. 56 (2022) 14808–14816, https://doi.org/10.1021/acs.est.2c04939.

[23] D. Wan, Y. Wang, Y. Liu, M. Gu, Y. Liu, S. Xiao, Q. He, Effect of nitrate and sulfate coexistence on hydrogen autotrophic reduction of antimonate (Sb(V)) and microbial community structures, Chemosphere 308 (2022), 136263, https://doi.org/10.1016/j.chemosphere.2022.136263.

[24] G. Zhang, X. Ouyang, H. Li, Z. Fu, J. Chen, Bioremoval of antimony from contaminated waters by a mixed batch culture of sulfate-reducing bacteria, Int. Biodeter. Biodegr. 115 (2016) 148–155, https://doi.org/10.1016/j.ibiod.2016.08.007.

[25] R. Deng, Y. Chen, X. Deng, Z. Huang, S. Zhou, B. Ren, G. Jin, A. Hursthouse, A Critical Review of Resistance and Oxidation Mechanisms of Sb-Oxidizing Bacteria for the Bioremediation of Sb(III) Pollution, Front. Microbiol. 12 (2021) 2418, https://doi.org/10.3389/fmicb.2021.738596.

[26] J. Li, Y. Zhang, S. Zheng, F. Liu, G. Wang, Anaerobic Bacterial Immobilization and Removal of Toxic Sb(III) Coupled With Fe(II)/Sb(III) Oxidation and Denitrification, Front. Microbiol. 10 (2019) 360, https://doi.org/10.3389/fmicb.2019.00360.

[27] Y. Zhu, M. Wu, N. Gao, W. Chu, N. An, Q. Wang, S. Wang, Removal of antimonate from wastewater by dissimilatory bacterial reduction: Role of the coexisting sulfate, J. Hazard. Mater. 341 (2018) 36–45, https://doi.org/10.1016/j.jhazmat.2017.07.042.

[28] L. Wang, L. Ye, C. Jing, Genetic Identification of Antimonate Respiratory Reductase in *Shewanella* sp. ANA-3, Environ. Sci. Tech. 54 (2020) 14107–14113, https://doi.org/10.1021/acs.est.0c03875.

[29] J. Li, Y. Liang, Y. Miao, D. Wang, S. Jia, C.-H. Liu, Metagenomic insights into aniline effects on microbial community and biological sulfate reduction pathways during anaerobic treatment of high-sulfate wastewater, Sci. Total Environ. 742 (2020), 140537, https://doi.org/10.1016/j.scitotenv.2020.140537.

[30] Y. Tang, C. Zhou, S.W. Van Ginkel, A. Ontiveros-Valencia, J. Shin, B.E. Rittmann, Hydrogen permeability of the hollow fibers used in H2-based membrane biofilm reactors, J. Membr. Sci. 407–408 (2012) 176–183, https://doi.org/10.1016/j.memsci.2012.03.040.
[31] Apha, Standard methods for the examination of water and wastewater, Apha, 1985.
[32] W. Li, M. Zhang, D. Kang, W. Chen, T. Yu, D. Xu, Z. Zeng, Y. Li, P. Zheng, Mechanisms of sulfur selection and sulfur secretion in a biological sulfide removal (BISURE) system, Environ. Int. 137 (2020), 105549, https://doi.org/10.1016/j.envint.2020.105549.
[33] H. Maeda, C. Fujimoto, Y. Haruki, T. Maeda, S. Kokeguchi, M. Petelin, H. Arai, I. Tanimoto, F. Nishimura, S. Takashiba, Quantitative real-time PCR using TaqMan and SYBR Green for Actinobacillus actinomycetemcomitans, Porphyromonas gingivalis, Prevotella intermedia, tetQ gene and total bacteria, FEMS Immunol. Med. Microbiol. 39 (2003) 81–86, https://doi.org/10.1016/S0928-8244(03)00224-4.
[34] B.S. Mirza, D.L. Sorensen, R.R. Dupont, J.E. McLean, New Arsenate Reductase Gene (arrA) PCR Primers for Diversity Assessment and Quantification in Environmental Samples, Appl. Environ. Microbiol. 83 (2017) e02725-16. https://doi.org/10.1128/AEM.02725-16.
[35] Y. Sun, E.A. Polishchuk, U. Radoja, W.R. Cullen, Identification and quantification of arsC genes in environmental samples by using real-time PCR, J. Microbiol. Methods 58 (2004) 335–349, https://doi.org/10.1016/j.mimet.2004.04.015.
[36] L. Wang, M. Yu, Y. Liu, J. Liu, Y. Wu, L. Li, J. Liu, M. Wang, X.-H. Zhang, Comparative analyses of the bacterial community of hydrothermal deposits and seafloor sediments across Okinawa Trough, J. Mar. Syst. 180 (2018) 162–172, https://doi.org/10.1016/j.jmarsys.2016.11.012.
[37] K.J. Livak, T.D. Schmittgen, Analysis of Relative Gene Expression Data Using Real-Time Quantitative PCR and the 2−ΔΔCT Method, Methods 25 (2001) 402–408, https://doi.org/10.1006/meth.2001.1262.
[38] L. Yang, S. Pang, J. Zhou, X. Li, M. Yao, S. Xia, Biological reduction and hydrodechlorination of chlorinated nitroaromatic antibiotic chloramphenicol under H2-transfer membrane biofilm reactor, Bioresour. Technol. 376 (2023), 128881, https://doi.org/10.1016/j.biortech.2023.128881.
[39] G. Muyzer, E.C. de Waal, A.G. Uitterlinden, Profiling of complex microbial populations by denaturing gradient gel electrophoresis analysis of polymerase chain reaction-amplified genes coding for 16S rRNA, Appl. Environ. Microbiol. 59 (1993) 695–700, https://doi.org/10.1128/aem.59.3.695-700.1993.
[40] R.C. Edgar, UPARSE: highly accurate OTU sequences from microbial amplicon reads, Nat. Methods 10 (2013) 996–998, https://doi.org/10.1038/nmeth.2604.
[41] R. Polack, Y.-W. Chen, N. Belzile, Behaviour of Sb(V) in the presence of dissolved sulfide under controlled anoxic aqueous conditions, Chem. Geol. 262 (2009) 179–185, https://doi.org/10.1016/j.chemgeo.2009.01.008.
[42] S. Ndongo, F. Cadoret, G. Dubourg, J. Delerce, P.-E. Fournier, D. Raoult, J.-C. Lagier, 'Collinsella phocaeensis' sp. nov., 'Clostridium merdae' sp. nov., 'Sutterella massiliensis' sp. nov., 'Sutturella timonensis' sp. nov., 'Enorma phocaeensis' sp. nov., 'Mailhella massiliensis' gen. nov., sp. nov., 'Mordavella massiliensis' gen. nov., sp. nov. and 'Massiliprevotella massiliensis' gen. nov., sp. nov., 9 new species isolated from fresh stool samples of healthy French patients, New Microbes New Infect. 17 (2017) 89–95.
[43] S. Wang, Y. Wang, P. Li, L. Wang, Q. Su, J. Zuo, Development and characterizations of hydrogenotrophic denitrification granular process: Nitrogen removal capacity and adaptability, Bioresour. Technol. 363 (2022), 127973, https://doi.org/10.1016/j.biortech.2022.127973.
[44] M.F. Carboni, S. Arriaga, P.N.L. Lens, Simultaneous Nitrification and Autotrophic Denitrification in Fluidized Bed Reactor Using Pyrite and Elemental Sulfur as Electron Donor, (2022). https://doi.org/10.2139/ssrn.4103133.
[45] L. Zhang, L. Zhang, D. Xu, Application of low-intensity ultrasound to enhance simultaneous nitrification/iron-based autotrophic denitrification, Biotechnol. Lett. 44 (8) (2022) 1001–1010.
[46] E. Mauch, L. Serra Moncadas, A.-S. Andrei, Complete Genome Sequence of an Uncultivated Freshwater Bacteroidota Lineage, Microbiol. Resour. Announc. 11 (2022) e00766–e00822, https://doi.org/10.1128/mra.00766-22.
[47] J.-H. Park, O. Choi, T.-H. Lee, H. Kim, B.-I. Sang, Pyrosequencing analysis of microbial communities in hollow fiber-membrane biofilm reactors system for treating high-strength nitrogen wastewater, Chemosphere 163 (2016) 192–201, https://doi.org/10.1016/j.chemosphere.2016.07.099.
[48] C. Shi, Y. Xu, M. Liu, X. Chen, M. Fan, J. Liu, Y. Chen, Enhanced bisphenol S anaerobic degradation using an NZVI–HA-modified anode in bioelectrochemical systems, J. Hazard. Mater. 403 (2021), 124053, https://doi.org/10.1016/j.jhazmat.2020.124053.
[49] A. Schwarz, M. Gaete, I. Nancucheo, D. Villa-Gomez, M. Aybar, D. Sbárbaro, High-Rate Sulfate Removal Coupled to Elemental Sulfur Production in Mining Process Waters Based on Membrane-Biofilm Technology, Front. Bioeng. Biotechnol. 10 (2022), 805712, https://doi.org/10.3389/fbioe.2022.805712.
[50] Q. He, Y. Liu, D. Wan, Y. Liu, S. Xiao, Y. Wang, Y. Shi, Enhanced biological antimony removal from water by combining elemental sulfur autotrophic reduction and disproportionation, Journal of Hazardous Materials 434 (2022), 128926, https://doi.org/10.1016/j.jhazmat.2022.128926.